Optical feedback implementation for polymer based tunable laser

Master's Thesis of

Tianwen Qian

at the Karlsruhe School of Optics & Photonics
in cooperation with Fraunhofer Heinrich-Hertz-Institut

Reviewer:	Prof. Dr. Bryce S. Richards
Second reviewer:	Dr. Ulrich W. Paetzold
Advisor:	David de Felipe Mesquida

July 2018 – December 2018

Karlsruhe Institute of Technology
Karlsruhe School of Optics & Photonics
Schlossplatz 19
76131 Karlsruhe | Germany

I herewith declare that the present thesis is original work written by me alone, that I have indicated completely and precisely all aids used as well as all citations, whether changed or unchanged, of other theses and publications, and that I have observed the KIT Statutes for Upholding Good Scientific Practice, as amended.

Karlsruhe, 30.12.2017

. . . . . .

(Tianwen Qian)

Abstract

The optical feedback introduced improvement on laser linewith and bandwidth has drawn a significant interest for the researchers.

In practice external feedback when coupled into the laser cavity through the output facet, causes a modification of the photon density. This perturbation leads to a fluctuation in the carrier density affecting the optical gain. Since the fluctuations of optical refractive index are directly related to the carrier density [11], the external feedback also introduces phase fluctuations. The interaction of the intensity and phase fluctuations makes the dynamics of the laser system under self-injection very complex leading to system instabilities and even chaos. [Kechaou, Grillot et al 2012]

As high-speed fiber-optic communication becomes increasingly important, so does the need to perform precision measurements on lasers and lightwave systems.

Contents

1. Introduction

The focus of this thesis is the study of the optical feedback effects on polymer-based tunable laser in order to improve its performance in linewidth and bandwidth. The tunable laser is constructed by a hybrid approach combining polymer-based photonic integrated circuits (PIC) and active Indium Phosphide (InP) components.

Coherent optical communication systems are gaining rapid importance because they allow to increase the speed (data rate) of transmission, by making use of the phase-predicatability of lasers with narrow spectral linewidth.

Semiconductor laser diodes with wide direct modulation bandwidth represent a relevant element to fulfill the continuously increasing need for low-cost optical communications systems with high bit-rate.

The directly modulated laser is a simple and reliable source for high speed optical information transmis- sion. It is especially useful in medium to short distance applications (e.g. local area networks and optical interconnects) where the excess pulse dispersion due to laser chirp is not a critical issue. The laser modulation response can in most cases be described with a three pole transfer function.' The modulation bandwidth is then determined by the maximum achievable resonance frequency, the damping of the resonance peak and possible additional parasitic-like effects due to contact parasitics or diffusion-limited transport through the separate confinement layers.' For FP-lasers and single section DFB-lasers it is found both theoretically and experimentally that the damping of the relaxation peak increases approximately linearly with the relaxation frequency squared and this relation leads to an ultimate limit of the modulation response that mainly is determined by the ratio between the nonlinear gain coefficient and differential gain coefficient of the active material.2 However, this is not true in DBR-lasers or inhomogenously pumped multi-section DFB-lasers where it can be shown that the dispersive effects of the Bragg grating can alter both the frequency of the relaxation peak and its damping.

For the design process a set of three masks is needed, corresponding to the electrode, waveguide and air trench geometry.

The goal of this work is to analyze and improve the characteristics of the laser under feedback condition. Parameters measured by different set-ups for the characterization are presented in **??**. The samples produced based on this work are then characterized using optical transmission and reflection measurements. The measurements of these lasers, consisting of testing the designs, the application of different tuning principals and tuning experiments, are presented.

2. Theory of Laser Coupled with Passive Cavity

Semiconductor lasers with external cavities exhibit a variety of dynamical phenomena, depending on key parameters, comprising feedback strength, feedback delay, pump current, feedback type, and laser nonlinearity [1]. Among all of them, the feedback sensitivity of laser diodes is governed essentially by the feedback parameters C, X and κ_{ext}. In order to correctly consider the feedback effect in our tunable DBR laser, a three-mirror laser model and its equivalent two-mirror Fabry-Perot cavity are considered in Figure 2.1.

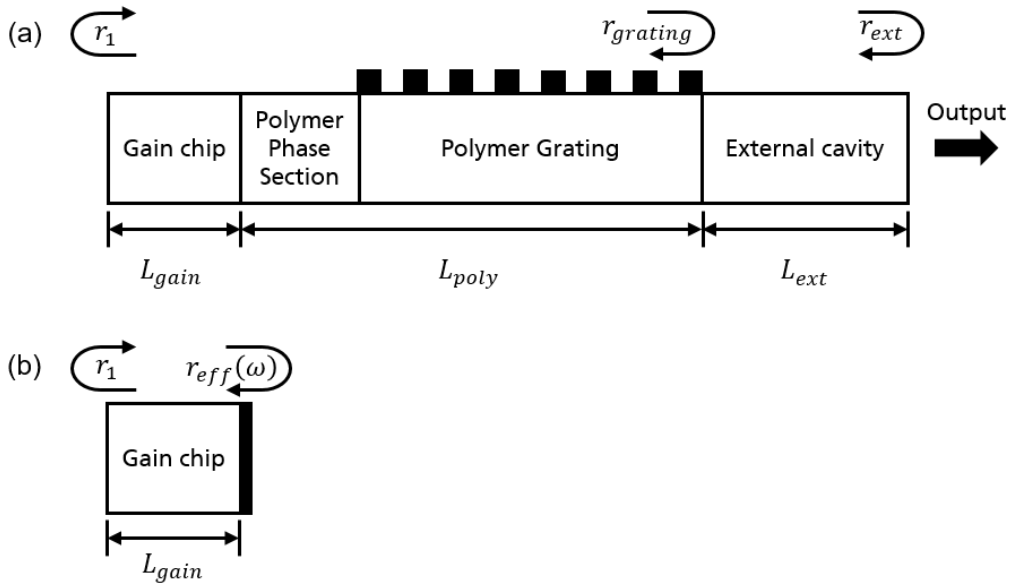

Figure 2.1.: (a) DBR laser with external cavity and (b) its equivalent cavity with effective mirror to model the feedback effect. The InP gain section that possesses a length of L_{gain} is equipped with a high reflection (HR) front facet and is but-coupled to the Polyboard. The Polyboard consists a phase and a grating section with a total length of L_{poly} and the external cavity with a length of L_{ext} after the grating section. r_1, $r_{grating}$ and r_{ext} are amplitude reflectivities of the gain chip front facet, grating and external reflector respectively.

The feedback coefficient, C, characterizes the level of feedback in relation to how it affects the mode structure of the laser, is defined as

$$C = X\sqrt{1+\alpha^2} \tag{2.1}$$

with

$$X = \frac{\tau_{ext}}{\tau_{gain} + \tau_{poly}} \kappa_{ext} \tag{2.2}$$

$$\kappa_{ext} = \frac{r_{ext}}{r_{grating}} \left(1 - \left|r_{grating}\right|^2\right) \tag{2.3}$$

where $\tau = 2nL/c$ is the roud trip time in the corresponding section, κ_{ext} is the coupling coefficient from the grating reflector to the external cavity and α is the linewidth enhancement factor. Note that here the grating reflectivity $r_{grating}$ is considered as a static value, which leads to effective grating length $L_{eff} = tanh(\kappa L)/2\kappa$ shorter than the real grating length L [2]. The L_{eff} is then contained in the normal cavity and the rest of the grating is included in the external cavity.

The C parameter indicates that the laser stability under feedback is affected both by external reflector r_{ext} and external round-time delay τ_{ext}. When $C < 1$, usually for weak feedback and relatively short external cavities, the laser operates in a single mode lasing region and is phase dependent to the external feedback, when $C > 1$, over one stable mode will appear and the laser will undergo a route-to-chaos behavior until it reaches coherence-collapse [3] region, which is the region IV for the experimentally identified five distinct regimes of laser performance under feedback [4]. After the coherence-collapse region, if the feedback strength is even higher, the laser will operates in stable single mode again lasing with the compound cavity mode.

It is useful to identify the static lasing behavior by using the C parameter, but in order to quantitatively model the laser under feedback, the equivalent two-mirror cavity by replacing the external feedback part with an effective mirror of reflectivity $r_{eff}(\omega)$ is considered

$$r_{eff}(\omega) = r(\omega)e^{-i\varphi(\omega)} = \frac{r_{grating}(\omega) + r_{ext}W}{1 + r_{grating}(\omega)r_{ext}W} \tag{2.4}$$

$$W = e^{-2\alpha_{poly}L_{ext}} e^{-2i\beta_{poly}L_{ext}} \tag{2.5}$$

where α_{poly} and β_{poly} are the propagation loss and the propagation constant of the external cavity respectively, $r_{grating}(\omega)$ is the frequency-dependent complex amplitude reflectance of the grating reflector [5].

The resonance equation G for the effective laser cavity model is then given by [6]

$$G = r_1 e^{-2i\tilde{\beta}_{gain}L_{gain}} r_{eff}(\omega) = |G|e^{i\varphi(\omega)} \tag{2.6}$$

with

$$\tilde{\beta}_{gain} = \beta + i\beta_i = \beta + \frac{i}{2}(g - \alpha_{in}) \tag{2.7}$$

where the real part $\beta = 2\pi n_{gain}/\lambda$ is the propagration constant inside the gain section, and the imaginary part consists of the modal gain g and the internal loss α_{in} in the gain medium [7]. Cavity modes are obtianed from Equation 2.6 for integer values of $\varphi/2\pi$; for the lasing mode m at threshold we get

$$|G(\lambda_m)| = G_m = 1, \ \varphi_m = 2m\pi \tag{2.8}$$

these two conditions allow to numerically find the lasing mode wavelength λ_m.

2.1. Linewidth and Chirp Reduction

Linewidth and chirp reduction due to the optical feedback is related to the factor F, which is defined as [8]

$$F = 1 + A + B \tag{2.9}$$

with

$$A = \frac{1}{\tau_{gain}} \frac{d\varphi_{r_{eff}}}{d\omega} \tag{2.10}$$

$$B = \frac{\alpha}{\tau_{gain}} \frac{d \ln r_{eff}}{d\omega} \tag{2.11}$$

$$\Delta\omega = \frac{\Delta\omega_0}{F} \tag{2.12}$$

$$\Delta\nu = \frac{\Delta\nu_0}{F^2} \tag{2.13}$$

where α is the linewidth enhancement factor, $\Delta\omega$, $\Delta\nu$ and $\Delta\omega_0$, $\Delta\nu_0$ are the chirp and linewidth with and without feedabck respectively. The parameter A is the freqeuncy derivative of the $r_{eff}(\omega)$ phase in Equation 2.4, it denotes the ratio of the effecitve round trip time (cavity path length outside gain medium) to the round trip time in the gain section (gain section path length). It can be interperated as the ratio of the photon numbers outside to inside the gain medium, which remains nearly constant once the laser cavity is formed. By designing a cavity with a long external cavity, a large A can be achieved. However, parameter B, representing the slope of the spectral reflectivity, is changed if the lasing mode is detuned. Additional reduction occurs only at the rising slope of the spectral peak of the external feedback which represents the contribution of the detuned loading effect and will be explained in Subsection 2.2.1.

Consider the five different feedback regions studied in [4], the reduction factor at weak feedback ($C < 1$) becomes [7, 9]

$$F = 1 + C\cos(\phi_{ext} + \arctan\alpha) \tag{2.14}$$

where $\phi_{ext} = 2\beta_{poly}L_{ext}$ is the round trip phase of the external cavity. Equation 2.14 shows that at weak feedback, the linewidth can either be narrowed $\Delta\nu_0/(1+C)^2$ or broadened $\Delta\nu_0/(1-C)^2$ depending on the feedback phase. For strong feedback, which is more interesting and stable for the practical implementation, the factor F becomes

$$F = 1 + f_{ext}\frac{\tau_{ext}}{\tau_{gain} + \tau_{poly}} \tag{2.15}$$

with

$$f_{ext} = \eta_{couple}R_{ext} \tag{2.16}$$

where η_{couple} is the coupling coefficient between the normal cavity and external cavity. This parameter is included because for the design presented in Section 4.1, the feedback from the external cavity is not totally coupled back to the normal cavity. However, in this case $\eta_{couple} = 1$.

With Equation 2.14 and Equation 2.15 we calculated the linewidth reduction factor F^2 versus the external cavity length as shown in Figure 2.2. L_c indicates the length when the C parameter goes over 1 and unstable laser behavior is expected. Figure 2.2 is caculated under the assumption that the feedback comes from the chip edge, which is formed by a polymer/air interface and results in $R_{ext} = 0.187$.

Table 2.1.: Parameters used for linewidth reduction factor F^2 calculation.

Symbol	Description	Value
L_{gain}	Active section length	300 μm
L_{phase}	Phase section length	525 μm
$L_{grating}$	Grating section length	699.84 μm
L_{poly}	Polymer section length	1224.84 μm
α	Linewidth redcution factor	-3
$R_{grating}$	Grating reflectivity	0.3
R_{ext}	External cavity reflectivity	0.187

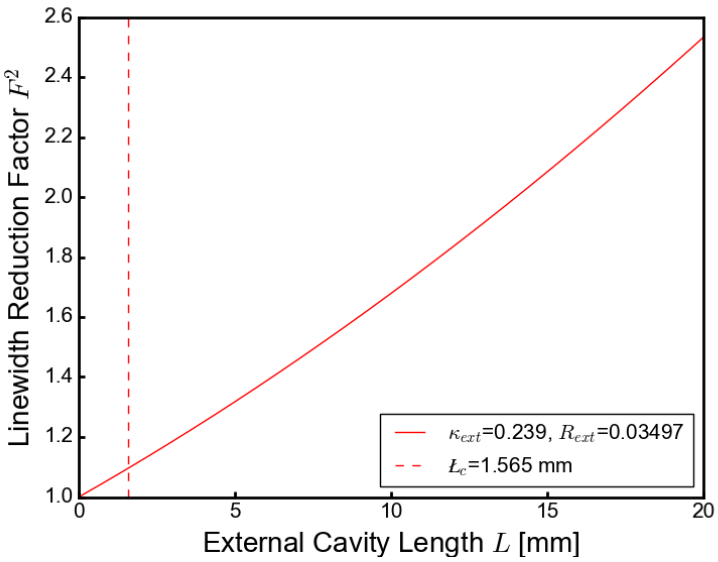

Figure 2.2.: Calculated linewidth reduction factor F^2 assuming the feedback comes from the poly/air interface. Dashed vertical line L_c indicates the length where the C parameter exceeds 1 and unstable laser behavior is expected.

2.2. Bandwidth Enhancement

The maximum bit rate achieved by direct modulated lasers is limited by the well known resonance between carriers and photons [7]. Many solutions have been proposed to over-

come this restriction and three approaches to achieve broader bandwidth are explored in detail here.

2.2.1. Detuned Loading Condition

The first mechanism identified to extend the modulation bandwidth of a semiconductor laser is the detuned loading effect which is due to the dispersion effect introduced by a coupled cavity [10, 11] or by a distributed mirror (e.g. DBR [12, 13, 14]). It can be achieved by positioning the lasing mode at a slightly higher wavelength respect to the minimum threshold gain condition, which means the lasing mode of a DBR laser is oscillating at the higher slope of its grating response. It is reported that when the laser is operating at the longer wavelength side, an enhancement of modulation speed, reduction of phase noise (linewidth), and suppression of FM modulation (chirping) can be achieved [10]. The detuned loading of the laser cavity increases the interaction between the photons and the free carriers in the laser cavity which will both increase the modulation bandwidth and reduce the variation of the carrier density during modulation [15]. This is because, in the longer wavelength region, the increase in carrier density increases the material gain while reducing the mirror loss (i.e. increase the reflection from the grating). As a result, the effective differential gain is increased, which, in turn, reduces the effective linewidth enhancement factor [10, 14].

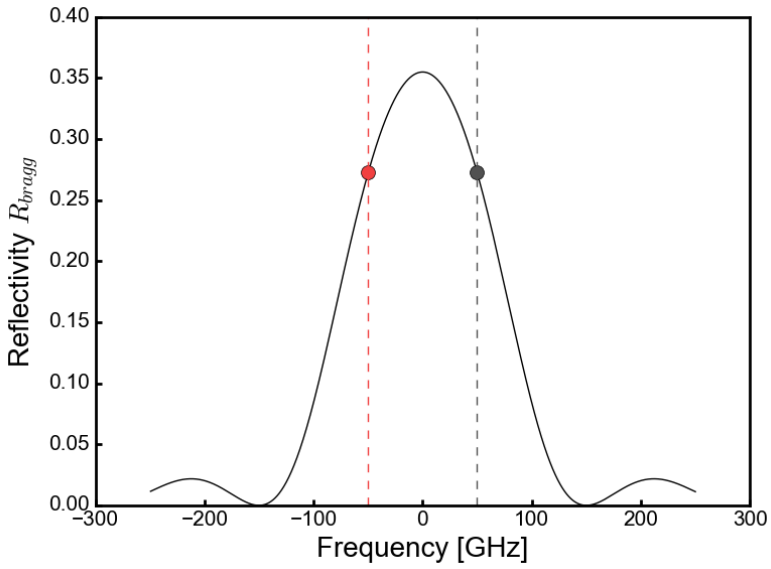

Figure 2.3.: Detuned loading condition with respect to the grating response. The red and grey dots correspond to the lasing mode detuend to the longer and shorter wavelength sides.

2.2.2. Undamped Relaxation Oscillation

Relaxation oscillation in a semiconductor laser occurs because the carrier cannot follow the photon decay rate. It usually smoothly decays out as long as the disturbance (e.g. external feedback) is small enough [16]. However, it can become undamped when the laser is influenced by strong feedback (e.g. from the chip facet), which affects the laser lorentzian lineshape that the undamping peaks appear beside the main mode with the mode spacing of relaxation frequency in the spectrum. The undamped relaxation oscillation occurs for the appropriate combinations of feedback phase and strength as shown in Figure 2.4. The satellite peaks first show up with low phase current, then slowly increase their intensity and move towards the main peak, followed by more satellite peaks appearing when the corresponding relaxation oscillation frequency is further decreased.

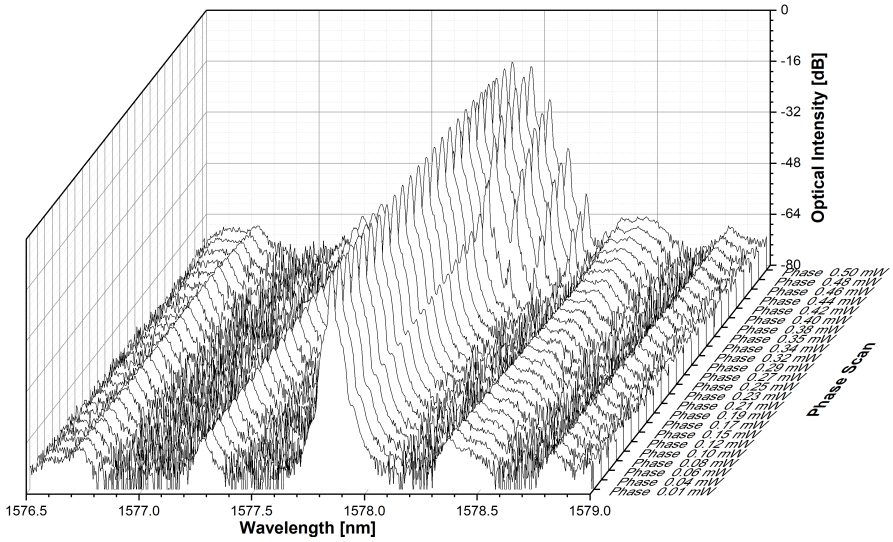

Figure 2.4.: Phase scan of the tunable DBR laser spectra with feedback from the chip facet. The side peaks of undamped RO start to appear, increase their intensity and shift toward the main peak. While the applied phase current keeps changing, more peaks develop until the laser shift to another mode and enters stable single mode lasing again.

Since the incoming feedback acts like a perturbation for the normal laser which introduces the amplitude modulation, the undamped RO can also be called as self-modulation and self-pulsation. The mechanism of self-pulsation is analysed and discussed in [17] as "dispersive Q-switching". In order to explain the self-pulsations one usually assumes some kind of Q-switching process, where the term Q-switching denotes a switching of the quality-factor of the laser cavity. If an increase of optical power yields a decrease of optical loss (or an increase of optical gain) within the laser, the round trip gain may become larger than unity, yielding an exponential increase of optical power, corresponding to the rising edge of a developing pulse. On the other hand an increased power yields an increasing consumption of carriers untile finally the carrier density is too low to maintain a unity round trip gain and therefore the optical power collapses. A recovery time is required in order to increase the carrier density again until the next pulse develops.

The repetition frequency for these pulses is of the same order as the relaxation resonance frequency [9]. The bandwidth enhancement by the self-pulsation effect has beed reported as a clear undamping of the relaxation peak which in some cases ultimately led to self-pulsations at the relaxation frequency is observed in the small signal modulation response of the laser. The increased relaxation frequency and the undamping of the relaxation peak can be utilised in order to achieve higher bandwidth [18].

2.2.3. Photon-Photon Resonance

Another approach used to extend the dynamic properties of an integrated laser, similar to detuned loading condition, in addition takes advantage of the interaction between the lasing mode and an adjacent longitudinal cavity mode, properly separated in frequency in such a way they can interact due to the carrier pulsation introduced by the applied modulation signal at the gain section. This interaction introduces a resonance in the impulse modulation (IM) response at the frequency corresponding to the mode separation. This resonance is frequently called Photon-Photon resonance (PPR), to distinguish this interaction mechanism respect to the Carrier-Photon resonance (CPR) [19]. The occurence of the PPR should not be too far away from the relaxation oscillation frequency so that the dip in between two peaks will not reach the -3 dB limitation in the modulation response as shown in Figure 2.5.

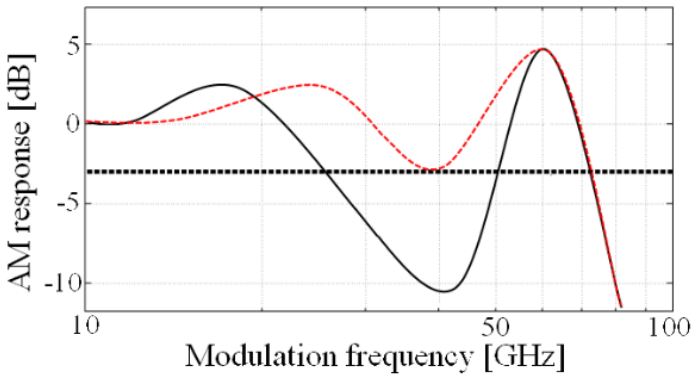

Figure 2.5.: Example of modulation responses obtained in a cavity exploiting the PPR effect. The black line indicates a case in which the CPR and the PPR peaks are too far whereas in the case indicated by the red line the modulation bandwidth extension is achieved [19].

The large enhancement of the modulation bandwidth, already has been observed to be closely related to a special behavior of the cavity Round Trip Phase (RTP) function [20], which is the phase factor $\varphi(\omega)$ in Equation 2.6. In order to illustrate the operation principle of the PPR, we did the calculation by assuming the simplified DBR laser structure as in [19], which contains only a gain section and a grating. Parameters used for this calculation are shown in Table 2.2 and the python code is provided in Section A.1.

The caculated result is shown in Figure 2.6, from which we can see the most favorable operation condition is when the lasing mode f_0 operates in the detuned loaidng condition

Table 2.2.: Simplified DBR laser cavity parameters used for calculation [19].

Symbol	Description	Value
L_A	Active region length	140 μm
L_G	Grating region length	780 μm
κ	Grating coupling coefficient	20 cm^{-1}
n_{eff}	Effective refractive index	3.7
R_R	Right side reflectivity	0
R_L	Left side reflectivity	0.32

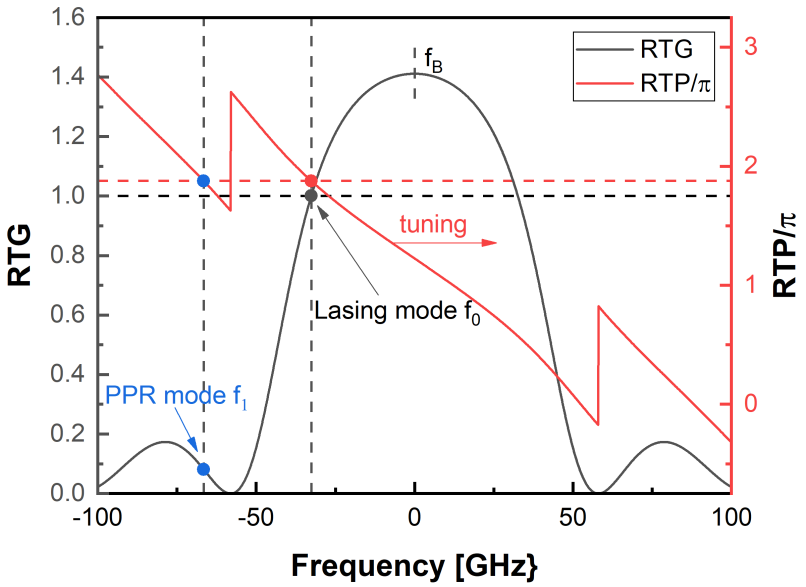

Figure 2.6.: Round trip gain (RTG, grey curve) and phase (RTP, red curve) functions computed at the DBR threshold. The grey and red marker represent the lasing mode f_0 at the corresponding RTG and RTP curve, the blue marker indicates the PPR mode f_1.

$f_0 < f_B$ and a mode f_1 on the same side with respect to the Bragg wavelength is placed on the the first lobe of the Round Trip Gain (RTG) curve. In this mode configuration, the PPR effect can arise due to the coupling between mode f_0 and f_1 [19], the corresponding PPR frequency is then the difference between the lasing mode f_0 and the PPR mode f_1. In order to generate an adjacent longitudinal cavity mode under feedback, a strong feedback condition is required, which will form compound cavity modes with the Free Spectral Range (FSR) considering the normal cavity plus the external cavity as defined in Equation 2.17

$$\Delta\nu = \frac{c}{2(n_{gain}L_{gain} + n_{poly}L_{eff})} \tag{2.17}$$

this equation is also used as the design guideline in Section 4.1.

3. Tunable Laser with Feedback from Chip Facet

Characterization of the normal tunbale DBR laser linewidth, RIN, bandwidth, α parameter and phase noise are measured with (1) Cleaved fiber with oil and (2) Lensed fiber, which corresponding to the laser without feedback and with feedback from chip facet conditions. Principle of each measurement will be introduced and the results will be compared in the following sections.

The measurements are done by fixing the gain section current at $I_{gain} = 80\ mA$, grating section current at $I_{grating} = 15\ mA$ and scanning the phase section from 0 mA to 30 mA with the step of 0.5 mA, each current step is considered as one index which leads to in total of 61 index numbers. The principle of phase scan and the observed spectra are shown in Figure 3.1 and Figure 3.3. By tuning the phase through the increasing current it shifts the cavity modes towards the shorter wavelength side, this effect is achieved by change of the effective refractive index inside the polymer waveguide which in turn changes the effecitve optical length of the cavity.

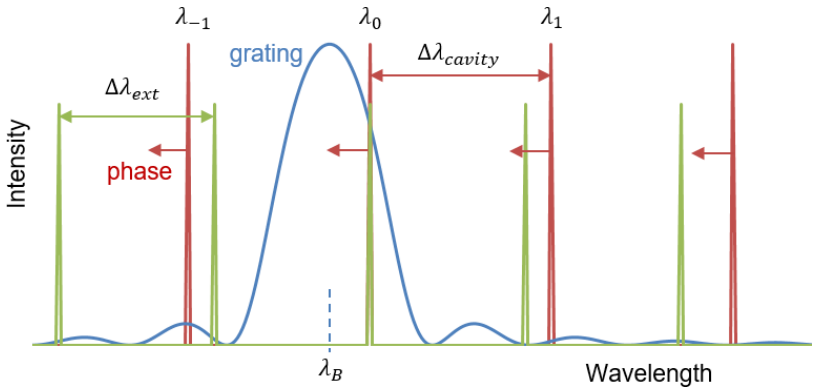

Figure 3.1.: Principle of phase scan in tunable DBR laser. Red and green curves represent the mode of the normal cavity and external cavity respectively. The different intensity is under the consideration that usually the feedback power is less than the output power. λ_0 is the lasing mode, λ_{-1} and λ_1 are its adjacent modes. λ_B is the Bragg wavelength which indicates the center of the grating response. $\Delta\lambda_{cavity}$ and $\Delta\lambda_{ext}$ are the mode spacing of the normal cavity and the external cavity. The red arrow indicates the phase shifts the cavity modes toward the shorter wavelength through the increasing phase current.

The scanning of the spectra and the examing of the Side Mode Suppression Ratio (SMSR) are shown in Figure 3.2. Due to the hysteresis effect the laser wavelength has

a little shift under these two configurations, e.g. the mode hopping point in Figure 3.2 a) appears at index 51 and the correspoinding point in Figure 3.2 (b) is at index 48. Besides, the additional hopping behavior in Figure 3.2 (b) is due to the feedback effect since the undamped RO peaks appearing in the spectra. Important to note that the light grey points marked at the beginning of Figure 3.2 (c) are unstable working points with SMSR lower than 40 dB, several modes appeared at these phase currents and the laser performance dropped drastically, which can be seen from the α parameter measurement in Section 3.4.

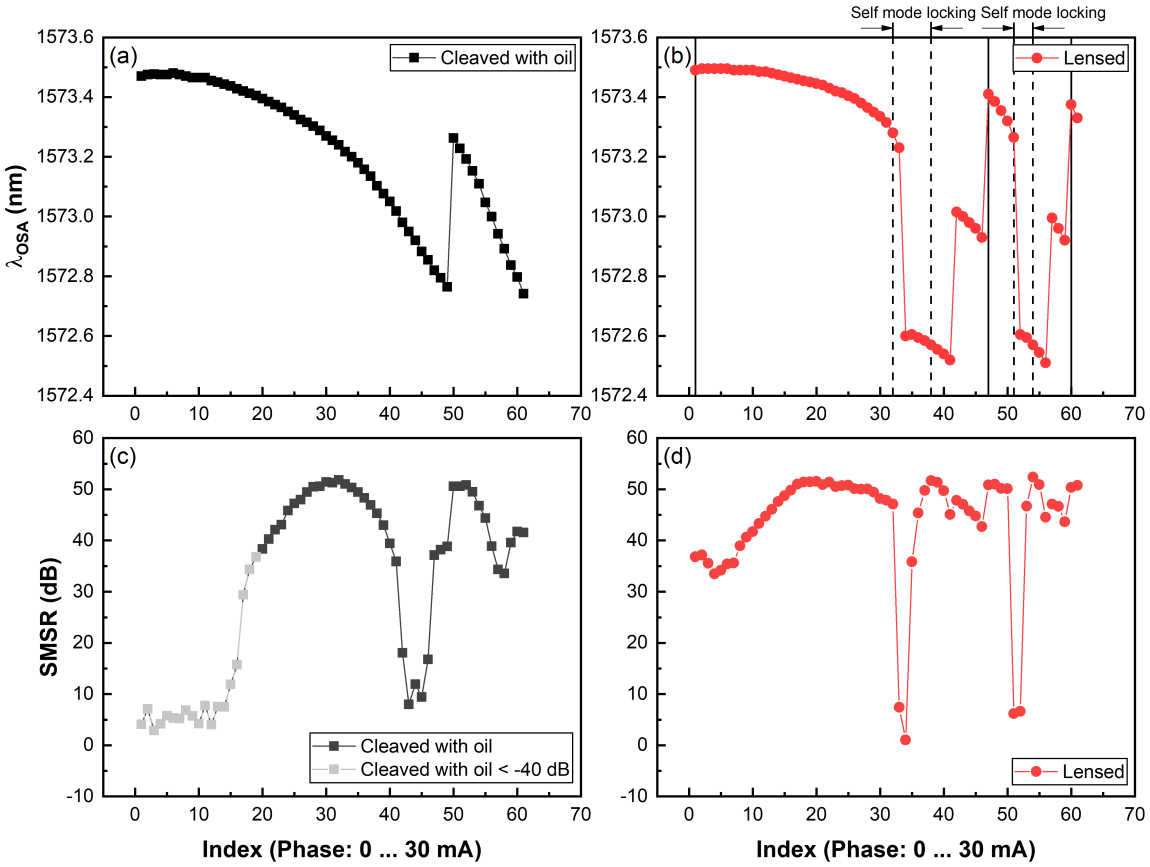

Figure 3.2.: Comparison of wavelength scanning (a), (b) and SMSR (c), (d) for tunbale DBR laser with feedback (red circled curve) and without feedback (black squared curve). (c) The light grey squared points at the beginning are unstable working points with several modes appearing and the laser performance dropped drastically. The other points which are lower than 40 dB are corresponding to the mode hopping behavior in the wavelength scan maps.

By using the parameters in Table 2.1 along with the external cavity formed between the end of the grating and the chip facet $L_{ext} = 1473.36\ \mu m$, we caculated the mode spacing for normal cavity and external cavaity as $\Delta\nu_{cavity} = 67.04\ GHz$ and $\Delta\nu_{ext} = 56.35\ GHz$ respectively. As seen from Figure 3.3 (a), the laser initially operates with the side mode of the external cavity, it is because with the feedback from the chip facet, the laser operates

in the relative strong feedback region with $C = 1.69$. While shifting the phase current, the undamped RO starts to appear as shown in Figure 2.4 and Figure 3.3 (b).

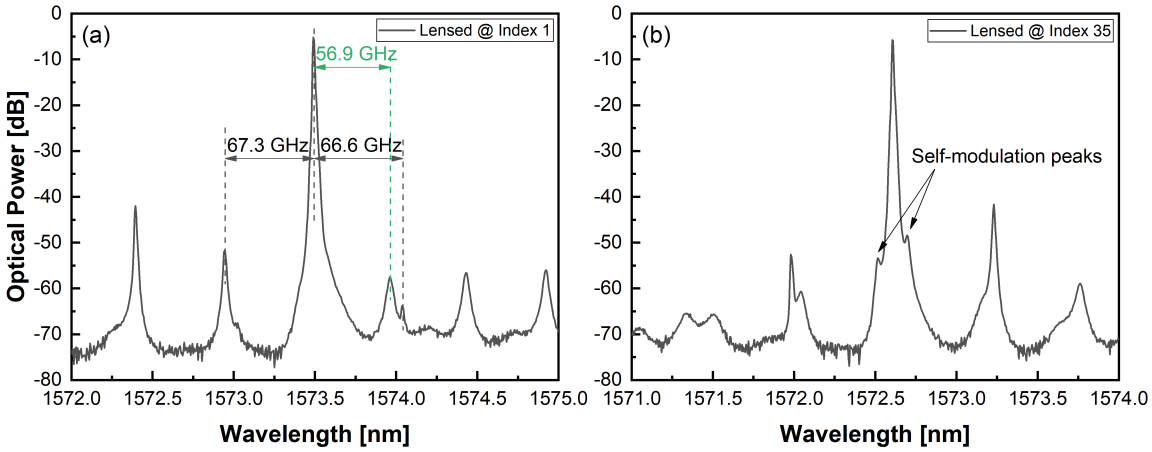

Figure 3.3.: Example of observed spectra for different phase current (index). (a) Green dashed line indicates the mode spacing between the main mode and the first side mode on the right, which corresponds to the normal cavity mode spacing $\Delta\nu_{ext} = 56.35\ GHz$, black dashed line indicates the mode spacing correspoinds to the external cavity $\Delta\nu_{cavity} = 67.04\ GHz$, (b) occurence of the self-modulation peaks on both sides of the main mode are pointed with black arrows.

Regarding to the cavity mode shifting behavior, we think the occurence of the self modulation peaks can be understood as a self mode locking behavior between the cavity mode and the external cavity mode, which is reported in [21]. In our case, we use this term to name the region where the undamped RO occurs, which is marked in Figure 3.2 (b), to seperate with the other lasing conditions along the phase shifting current.

3.1. Linewidth Measurement

Laser linewidth is measured by self-homodyne method in the characterization. Self-homodyning can be described mathematically as a single-delay autocorrelation, which is shown in Figure 3.4, the optical spectrum at f_0 autocorrelates with the delayed version of itself to produce a time-fluctuating spectrum, whose detected voltage has a power spectrum centered at zero frequency. For the case of a laser with Lorentzian lineshape, the half-width of the detected spectrum is equal to the linewidth of the laser.

The self-homodyne measurement set-up is shown in Figure 3.5. The input directional coupler of the interferometer splits the light from the laser into two paths. One path is delayed in order to decorrelate the combinning signals, P_1 and P_2. The output coupler combines the two signals, which are then mixed at the photodectector of the lightwave signal analyzer. The homodyne power spectrum is then observed on the analyzer from

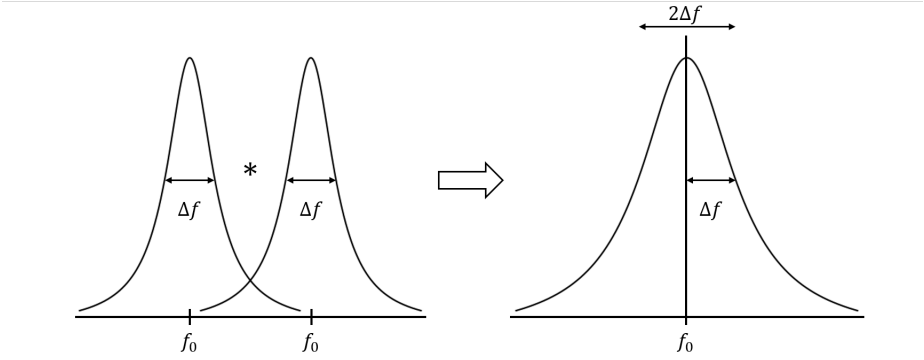

Figure 3.4.: Linewidth of a DBR laser using the self-homodyne technique. The optical spectrum at f_0 autocorrelates with the delayed version of itself to produce a time-fluctuating spectrum, whose detected voltage has a power spectrum centered at zero frequency, the half-width of the detected spectrum is equal to the linewidth of the laser.

which the Lorentzian linewidth is measured by placing a marker at the half power frequency.

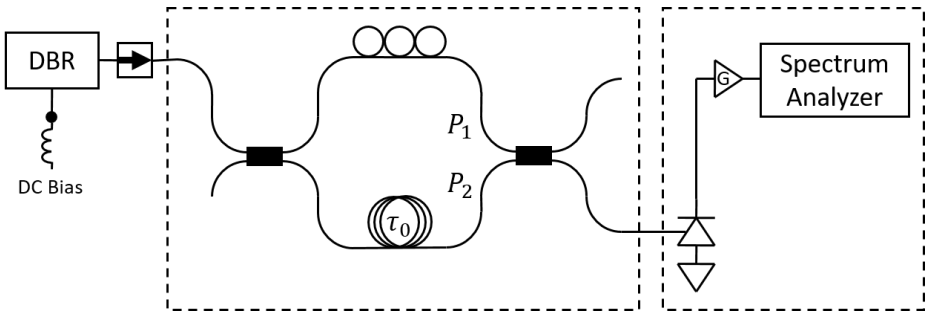

Figure 3.5.: Schematic set-up for self-homodyne linewidth measurement.

The results of linewidth measurement are shown in Figure 3.6. Except for the unstable working points which are shown in light grey squares in Figure 3.6 (a), the laser linwidth under feedback shows a more stable transition and become narrower than the case without feedback. It is due to the reason that the external refelctor formed by the polymer/air interface with $C = 1.69$ is considered to be in the relative strong feedback region. In such case, the practical formula for linewidth reduction factor F^2 Equation 2.15 has to be considered. The comparison for the lowerest linewidth for two configurations, along with the theoretical predcition, is shown in Table 3.1.

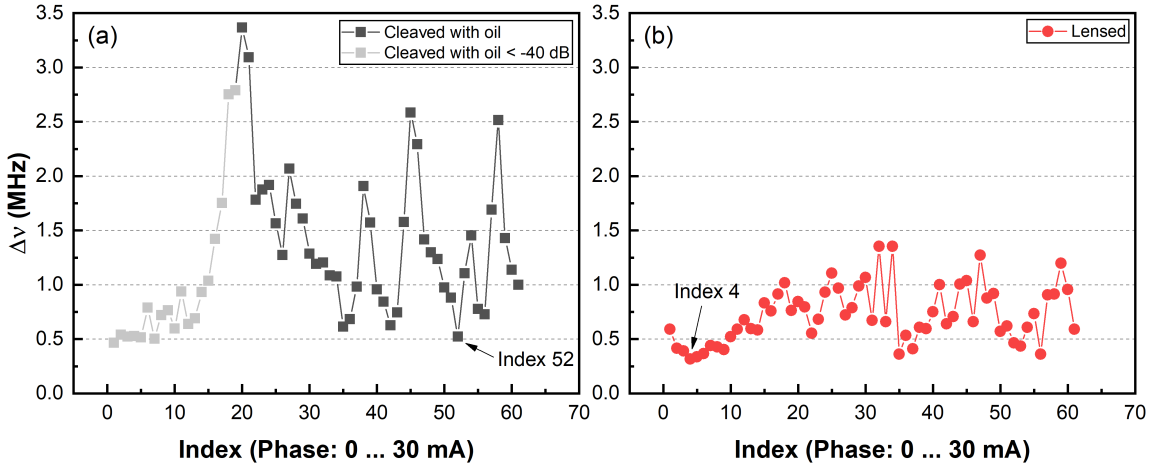

Figure 3.6.: (a) The laser linewidth without feedback from the chip facet, the light grey points indicate the bad working points, (b) laser linewidth with feedback from the chip facet, it appears to be more stable compare to the laser without feedback. The achieved lowest linewidth point are pointed with black arrow in each case.

Table 3.1.: Comparison between the linewidth reduction value achieved by laser w/ and w/o feedback and the predicated reduction value.

	w/o feedback	w/ feedback	Linewdith reduction factor F^2	
			Measured	Predicated
$\Delta\nu(MHz)$	0.522 @ Index 52	0.317 @ Index 4	1.647	1.11

3.2. Relative Intensity Noise (RIN) Measurement

The measurement of relative intensity noise (RIN) describes the laser's maximum available range for signal modulation and serves as a quality indicator of laser devices. RIN is defined as the ratio of the mean-square optical intensity noise to the square of the average optical power [9]

$$RIN = \frac{\langle \Delta P \rangle^2}{\langle P \rangle^2} dB/Hz \tag{3.1}$$

where $\langle \Delta P \rangle^2$ is the mean-square optical intensity fluctuations (in a 1-Hz bandwidth) at a specified frequency, and $\langle P \rangle$ is the mean optical power.

In order to measure the RIN, the optical power is converted to a current after the receiving photodiode and the ratio of optical powers squared is equivalent to the ratio of the detected electrical powers. Thus, RIN can be expressed in terms of detected electrical powers. Equation 3.1 can be rewritten as

$$RIN = \frac{N_{elec}}{P_{avg}(elec)} dB/Hz \tag{3.2}$$

where N_{elec} is the power-spectral density of the photocurrent at a specified frequency, and $P_{avg}(elec)$ is the average power of the photocurrent.

The noise at the receiver output results from three fundamental contributions: laser intensity noise primarily due to spontaneous light emissions; thermal noise from the electronics; and photonic shot noise. Since the photonic shot noise and the receiver thermal noise are not included in the definition of N_{elec}, they have to be subtracted from the measured RIN results

$$N_{laser} = N_{elec} - N_{shot} - N_{thermal}\ W/Hz \tag{3.3}$$

By using Equation 3.2 and Equation 3.3, the value of RIN_{laser} can be determined

$$RIN_{laser} = RIN(measured) - \frac{2e}{I_{avg}} - \frac{N_{thermal}}{P_{avg}(elec)} \tag{3.4}$$

where e is the elementary charge, I_{avg} denotes the detected average photocurrent, $N_{thermal}$ is the measured noise floor of the lightwave signal analyzer in a 1-Hz bandwidth.

The RIN comparison for the two configurations are shown in Figure 3.7. The RIN value for laser w/o feedback ranges from $-144.086\ dB/Hz$ to $-141.507\ dB/Hz$ while for lase with feedback it has two parts: without the spikes it ranges from $-146.283\ dB/Hz$ to $-140.216\ dB/Hz$, which is lower than the case without feedback; the spikes appear in Figure 3.7 (b) are correspoinding to the additional mode hopping behavior in Figure 3.2 (b), which indicates the appearing of the undamped RO, will increase the RIN value.

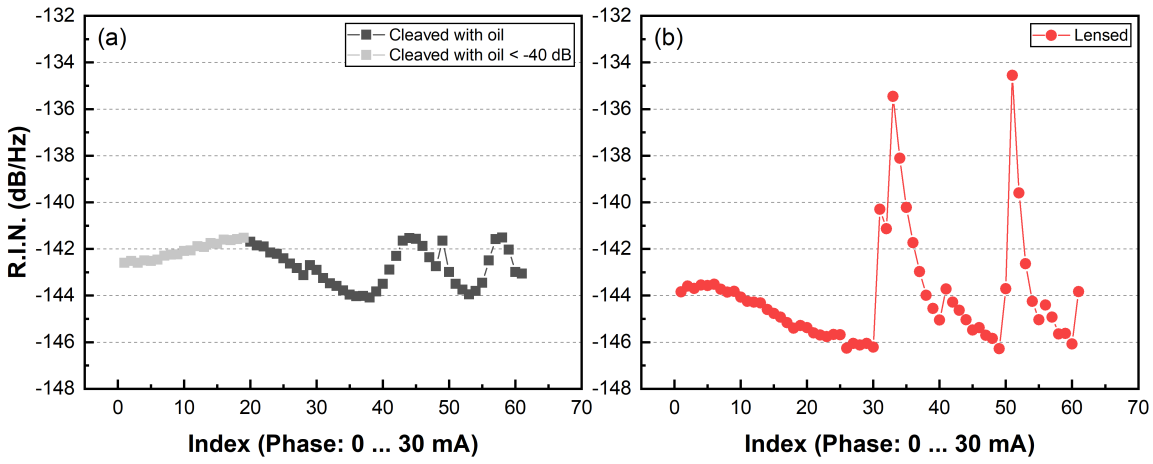

Figure 3.7.: Comparison of the RIN value for laser w/ and w/o feedback. (a) Laser with feedback, (b) laser without feedback, the spikes indicate the appearing of the undamped RO, which increase the RIN significantly.

3.3. Bandwidth Measurement

Measurement of the bandwidth by small signal modulation is presented as well as the bandwidth enhancement by detuned loading condition and the undamped relaxation oscillation.

3.3.1. Small Signal Modulation

The frequency response of a laser transmitter under small signal modulation is found by the usual assumption of a harmonic current modulation superimposed on a constant bias above threshold [R. Tucker 1985]. The modulation bandwidth f_{3dB} is a measure of the maximum modulation ability in semiconductor lasers through the injection current. It is usually defined as the frequency at which the modulation response has dropped by 3 dB relative to its zero freqeuncy value [16, 22]. The characteristics of the small signal modulation in a normal laser are mainly determined by the relaxation oscillation frequency f_r, which indicated by the position of the peak in the modulation response. Comparision of the bandwidth measurements for our tunable DBR laser is shown in Figure 3.8. Without feedabck, the increase of the relaxation oscillation freqeuncy f_r along with rising of the gain current is observed and the intensity drop is due to the higher damping facor achieved at the higher gain current. The maximum bandwidth achieved is 8.7 GHz. However, our DBR laser operates differently with feedback, the intensity of the relaxation oscillation peak got enhanced at gain value I_{gain} between 60 mA and 70 mA, in this case the maximum achieved bandwidth is 12.5 GHz. The reason for the enhancement of the bandwidth will be further studied in Subsection 3.3.2 and Subsection 3.3.3.

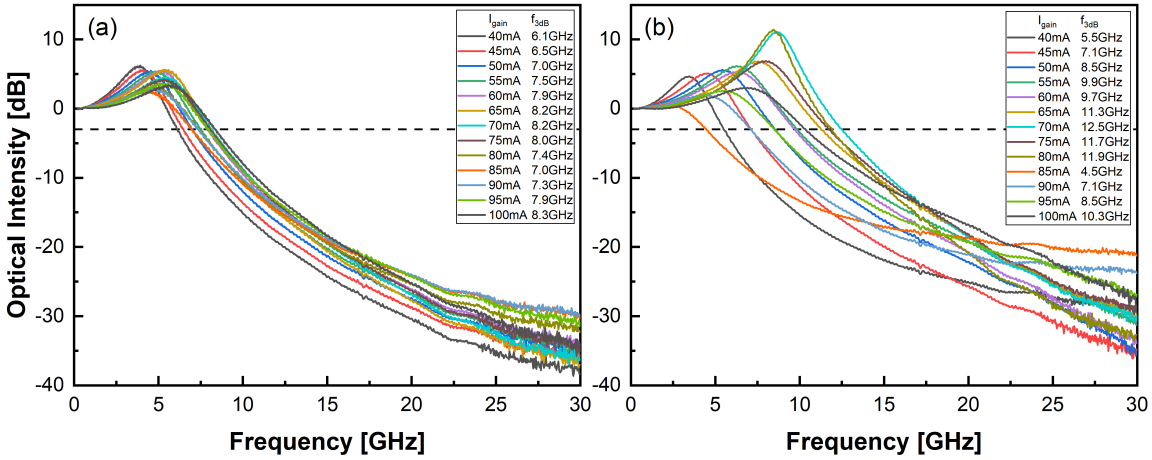

Figure 3.8.: Bandwidth measurements of a normal tunable DBR laser. (a) Without feedback, the f_{3dB} show a normal behavior that first increase with the applied gain current and then decrease, (b) with feedback, the prominant peaks at 70 mA and 75 mA are due to the undamped RO peaks, at this condition, the f_{3dB} got increased compare with the lase without feedback.

3.3.2. Detuend loading condition

Operating the tunable DBR laser under the detuned loading condition was measured without feedback and the result is shown in Figure 3.9. The measurement was performed by stabilizing the device at 25 °C and using a gain current $I_{gain} = 75\ mA$. When the laser is lasing on the slope of the grating response, the side modes have a different gain spectrum

relative to the peak of the grating response, which introduces the asymmetric behavior of the side modes. In this case, when the left side mode is higher than the right one, means the lasing mode is operating at the longer wavelength side of the grating response, and vice versa. By increasing the phase current I_{phase} from 14 mA to 20 mA, the lasing mode is tuned from the longer wavelength side of the grating response to the shorter wavelength side. The maximum f_{3dB} achieved at the longer wavelength side (red curve) is 10.6 GHz and the minimum (grey curve) is 8.5 GHz. These two operating points also correspoinds to the red and grey points in Figure 2.6. By exploiting the detuned loading effect with the best parameters from Figure 3.8 (a), the maximum achievable bandwidth is still 2 GHz lower than the one achieved by feedback, which means the enhancement in Figure 3.8 (b) is achieved not purely by detuned loading conditon without feedback effects.

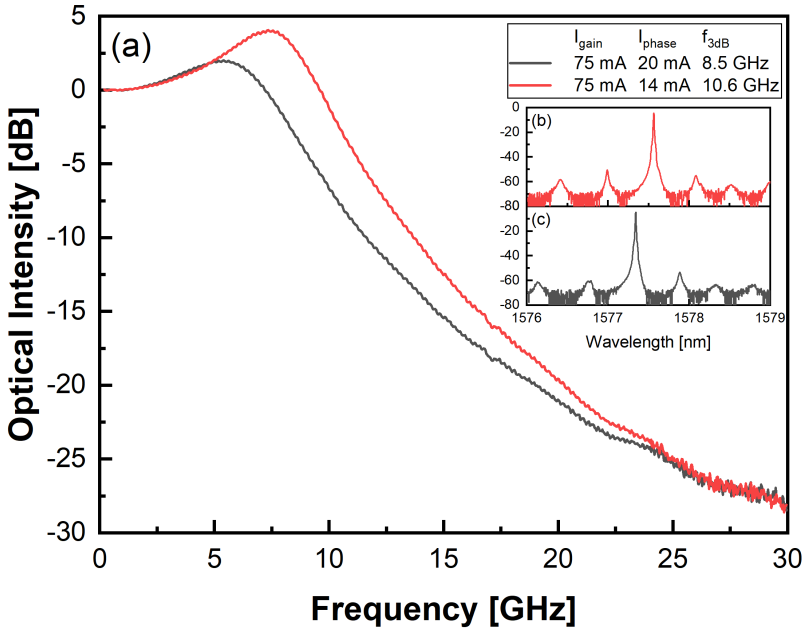

Figure 3.9.: (a) Bandwidth enhancement with the detuned loading condition on DBR tunable laser. The red curve is detuned to the longer wavelength side of the grating response and it shows an increased bandwidth of 2.1 GHz compared to the grey curve without bandwidth enhancement effect, (b) spectrum when laser operates at longer wavelength side, (c) spectrum when laser operates at lower wavelength side.

3.3.3. Undamped Relaxation Oscillation

The feedback from the chip facet behaves as a perturbation for the normal tunable DBR laser which leads to undamped RO conditons with different phase conditions. The measurements were performed with the same setting as in Subsection 3.3.2 and Figure 2.4, the results are in Figure 3.10. The appearing of the undamped RO peak leads to the carrier-photon resonance appears at a higher relaxation oscillation frequency which permits a higher f_{3dB} value of 14.6 GHz. As the side peaks slowly move towards the main peak

with increasing intensity, the carrier-photon resonance become stronger with a slightly decreased relaxation oscillating frequency which leads to a f_{3dB} value of 14.0 GHz. As more side peaks appear in Figure 3.10 (e), the undamped RO behavior is very strong which lead to a broder lineshape and the intensity modulation shows prominent peaks with frequency correspoinding to the mode spacing of the side peaks. This last behavior leads to broadened lineshape and significantly decreases the f_{3dB} compare to the other two cases. The increase of the relaxation oscillation intensity and the enhancement of bandwidth shown in Figure 3.8 (b) is certainly related to the occurence of the side peaks as shown in Figure 3.10 (a)-(d).

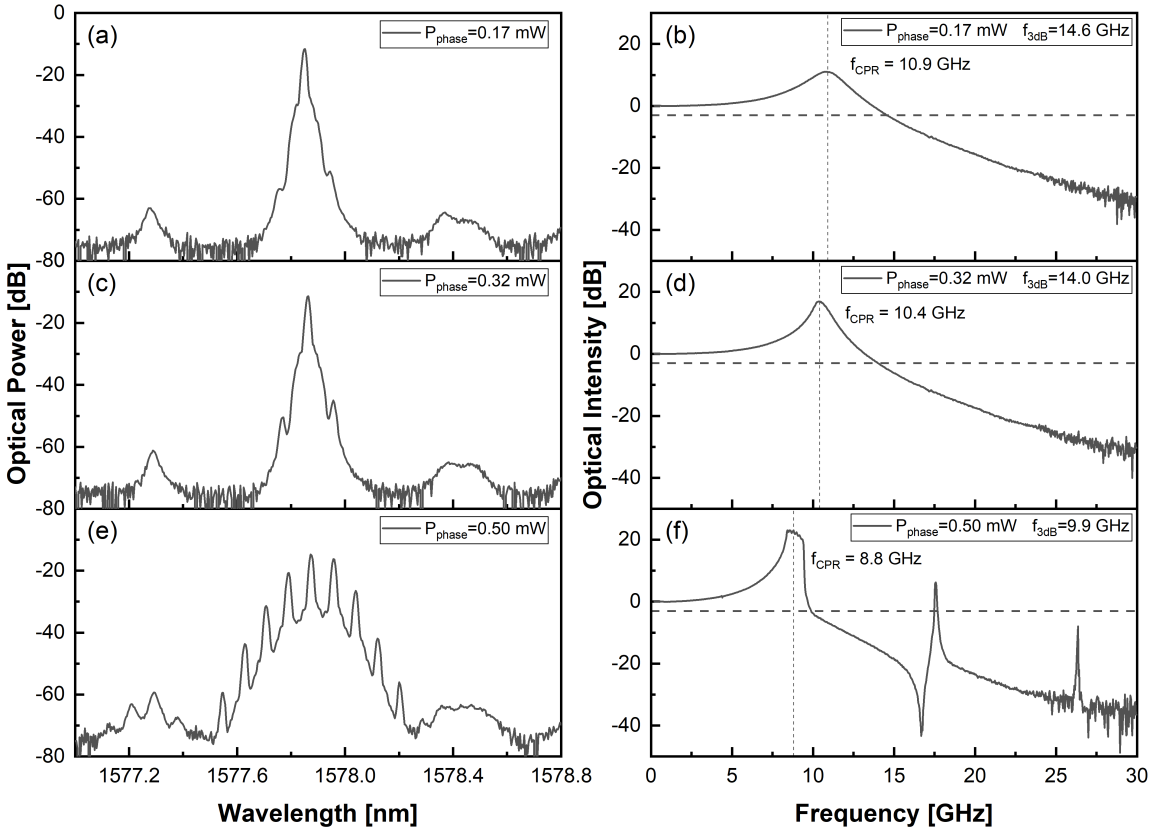

Figure 3.10.: Laser spectra and their correspoinding intensity modulation curve. (a) Appearing of the undamped RO peak leads to a higher carrier-photon resonance in (b), (c) growing of the side peaks leads to increase of the carrier-photon resonance peak in (d), (e) drastic undamped RO leads to broadened lineshape and decreased modualiton bandwidth in (f).

3.4. Chirp Parameter Measurement

Light chirping can be defined as the instantaneous change of the central wavelength or optical frequency in response to variations in the optical power. Two main contributions

of the frequency chirp are distinguished, one is a transient chirp component that evolve with the time deriative of the optical power, and is scaled by α, normally called linewidth enhancement factor when dealing with lasers. Another one is an adiabatic chirp, producing a frequency shift proportional to the instantaneous optical power, and scaled, in addition to α, by parameter κ, which is associated to the nonlinear gain [23, 24]. Here only the transient chirp is considered.

3.4.1. Measurement with Lightwave Component Analyzer

The network analyzer of Figure 3.11 measures the small signal frequency response of a light emitter, a dispersive medium and a light receiver. The dispersive medium is a standard single mode fiber of 81 km and an Er-doped fiber amplifier pumped at 1.55 μm. Resonance frequencies are observed as sharp peaks in the frequency response.

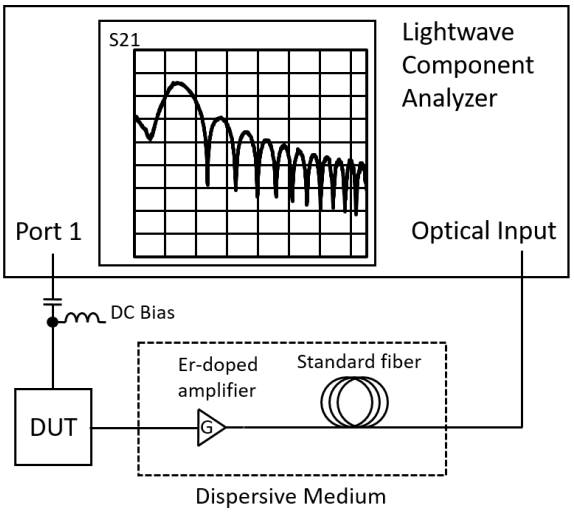

Figure 3.11.: Schematic set-up for chirp parameter measurement using Lightwave Component Analyzer.

The output optical intensity is assumed as [25]

$$I = I_0(1 + mcos(2\pi ft)) \qquad with\ m \ll 1 \tag{3.5}$$

with m being the modulation depth and f the modulation frequency of light intensity. The frequency response which is measured by the set-up described above is then [25]

$$I_f = I_0 m\sqrt{1+\alpha^2}\left|\cos\left(\frac{\pi\lambda^2 DLf^2}{c} + \arctan(\alpha)\right)\right|. \tag{3.6}$$

The resonance frequencies f_u (as shown in Figure 3.12 (a), (c)) correspond to the u^{th}-zeros of Equation 3.6. They follow the following equation [25]

$$f_u^2 L = \frac{c}{2D\lambda^2}\left(1 + 2u - \frac{2}{\pi}arctan(\alpha)\right) \tag{3.7}$$

which is the result of two simultaneous interferences between the carrier and the two sidebands. Plotting $f_u^2 L$ versus $2u$ gives a straight line whose slope and position yield the dispersion and the chirp parameter by linear regression. The frequency of the first dip is determined primarily by α, and to a lesser extent by D, whereas the frequency of the second dip is determined primarily by D and to a lesser extent by α, D is the fiber dispersion coefficient [26].

The frequency response form LCA and fitted linear regression data are shown in Figure 3.12, the obtained α parameter in two conditions is compared in Table 3.2. The deviated α parameter at 80 mA with a value of 4.13 can be clearly seen from Figure 3.12 (c), whereas the position of the first dip of the purple curve which indicates 80 mA is deviaited from the other current values, we think it may come from the effect of undmaped RO since in Figure 3.8 (b) at 80 mA the self modulation introduced increase of relaxation oscillation peak appears. Except for this current value, the achieved α parmaerters with feedback are generally lower than the without feedback case. The different calculated F factor may come from shifting of the phase by increasing the current value.

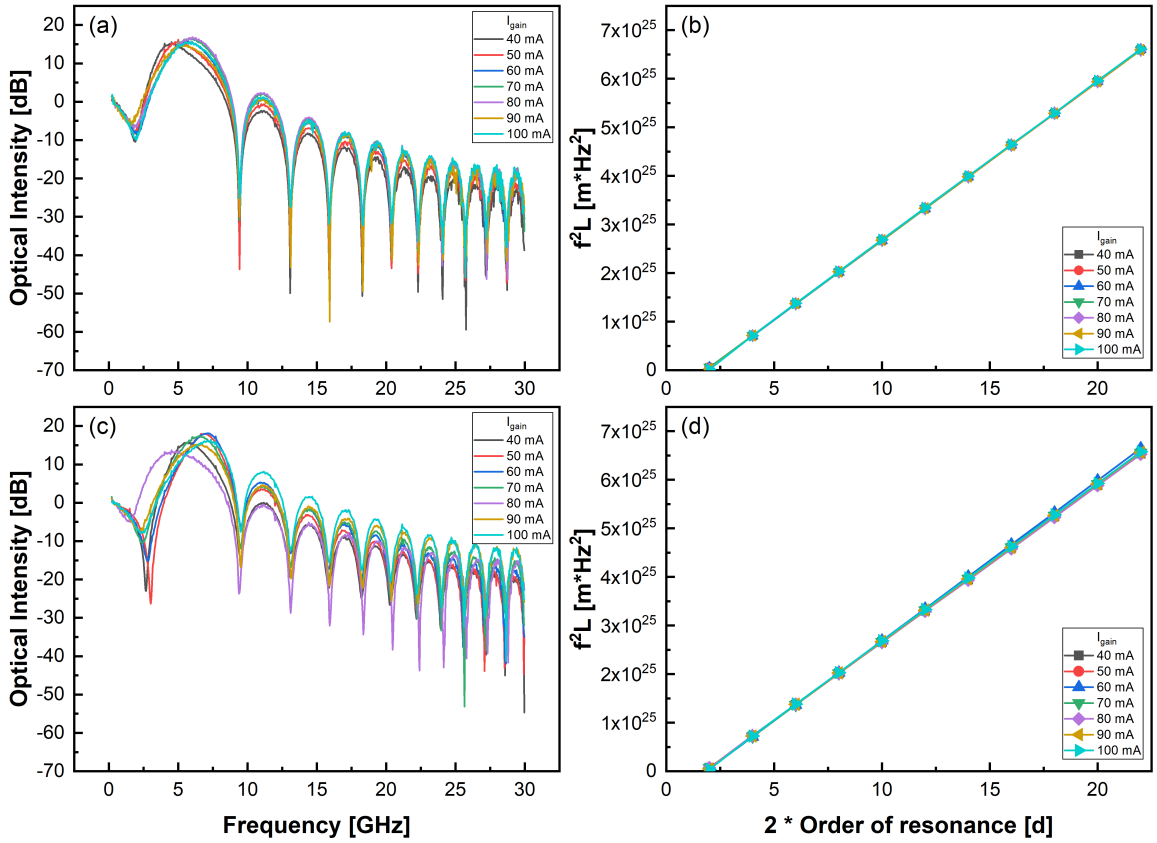

Figure 3.12.: Frequency response from the LCA measurement, (a) without feedabck, (c) with feedabck. Resonance frequencies squared (x-axis of (a) and (c)) times fiber length (81 km) versus two times the order of the resonance, (b) without feedback, (d) with feedback. Linear regression allows to find the chirp parameter and the dispersion from Equation 3.7.

Table 3.2.: Comparision of achieved α parameter value. Laser with feedback in general shows a decreased α value at all current values except for 80 mA. The different calculated F factor may come from shifting of the phase by increasing the current value.

Current [mA]	α		F
	w/o feedback	w/feedback	Chirp reduction factor
40	3.904	2.768	1.410
50	3.771	2.383	1.582
60	3.336	2.658	1.255
70	3.837	2.998	1.280
80	3.756	4.13	0.909
90	3.97	2.934	1.353
100	3.299	2.912	1.133

3.4.2. AM-FM Index Method

Transient chirp parameter α can also be obtained from measurements of the optical intensity spectrum. For this measurement technique, the ratio of residual phase modulation to amplitude modulation is measured from the optical spectrum of the laser when it is modulated with a sinusoidal signal of frequency f, the output optical intensity is assumed same as Equation 3.5. The optical intensiy spectrum of this signal is characterized by and optical carrier with power I_0, and two first oder sidebans with average power given by [24]

$$\overline{I_{\pm 1}} = I_0\left(\frac{m}{4}\right)^2\left(1 + \left(\frac{2p}{m}\right)^2\right) \qquad with\ m \ll 1 \tag{3.8}$$

where p is the phase modulation index [24], which is related to the transient and adiabatic chirp parmaerters by [27]

$$\frac{2p}{m} = \alpha\sqrt{1 + \left(\frac{f_c}{f}\right)^2} \tag{3.9}$$

where f_c is the chirp frequency. For modulation frequencies $f \gg f_c$, Equation 3.9 results to [24]

$$\frac{2p}{m} = \alpha \tag{3.10}$$

By measuring the power in the carrier and the sidebands from the optical spectrum the paratmeter p can be obtained, the value of m can be obtained from the instanteneous power signal, therefore α parameter is characterized [24, 23].

The α parameter measurement results are shown in Figure 3.13. Lower α value is achieved for laser with feedback with value of -1.208 compare to the without feedback with value of -2.36. For laser with feedback the α parameter value ranges from -4.581 to -1.208 where as for laser without feedback it is from -4.944 to -2.36. It shows a similar result as the method in Subsection 3.4.1, with which we can confirm the α parameter under feedback conditions is decreased.

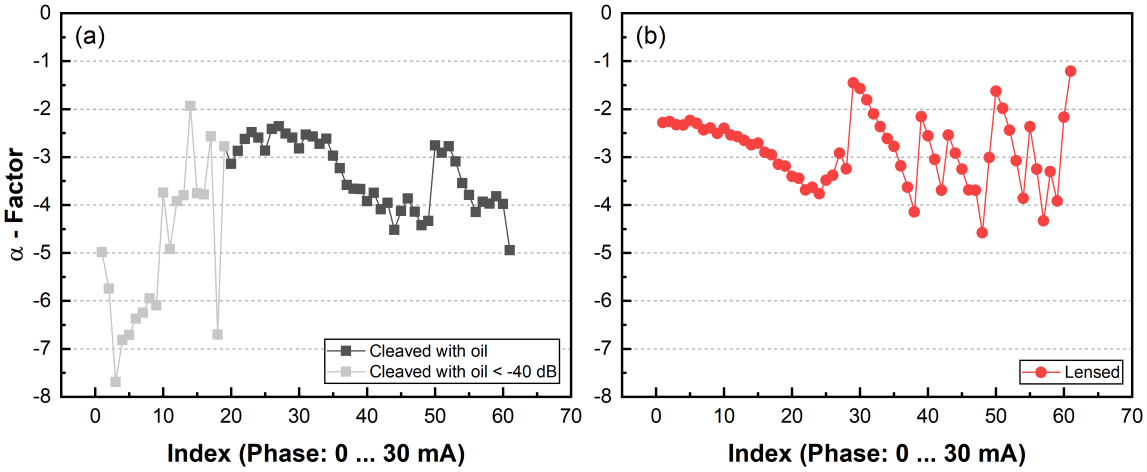

Figure 3.13.: (a) Measurement with cleaved fiber with oil, the light grey squares are corrospoinding to the unstable points mentioned before, (b) measurement with lensed fiber, lower α parameter value is achieved.

3.5. Phase Noise Measurement

4. Tunable Laser with on Chip Controllable Feedback

4.1. Design

The design of the on chip controllable feedback is targeting to the region I (phase dependent linewidth reduction) and region V (strong feedback with coumpound cavity mode) in the studied five feedabck regions [] by ustilization of the Bragg grating, Multimode Interferometer (MMI), Variable Optical Attenuator (VOA) and Thin Film Filter (TFF) structures on our Polyboard platform.

4.1.1. Active and Passive Elements

The grating is designed to have its Bragg wavelength at $\lambda_B = 1550\ nm$. Variable Optical Attenuator (VOA) is acheived with a 1×1 thermally tunable MMI by placing an electrode on the side along the MMI which allows the thermo-optical effect. Thin Film Filter (TFF) acts as a high reflectivity mirror with its operating wavelength covers the grating Bragg wavelength, it can be simply inserted in the TFF slot thanks to our Polyboard technology. The characterization example of the VOA is shown in Figure 4.1. Maximum $-28.39\ dB$ damping was achieved at current value of 54 mA.

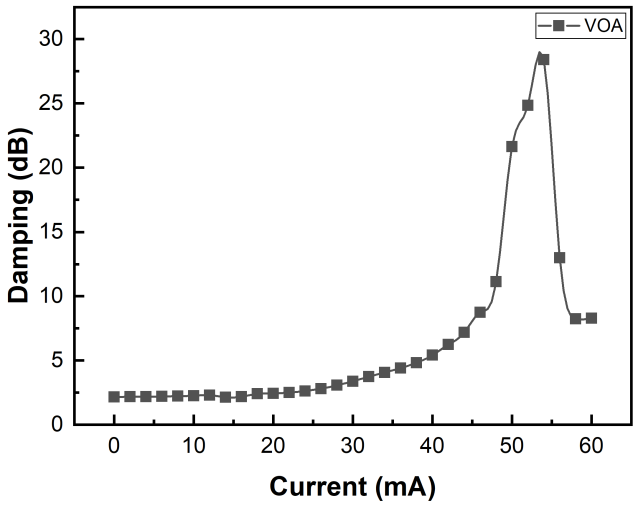

Figure 4.1.: Characterization of the VOA with maximum $-28.39\ dB$ damping achieved at current value of 54 mA.

4.1.2. Long Feedback Cavity

The on-chip long feedback cavity design is achieved by the spiral structure with the bending radius of 1500 μm. The beginning of the chip is our normal tunable laser, followed by a 1×2 MMI to seperate the output port and the external cavity. In the external cavity, two VOA structures and a phase section is included. The spiral structure has a variable design to achieve external cavity length of [39.28, 55.70, 81.33, 86.53, 100.75, 157.35] mm. By using Equation 2.14 and Equation 2.15 The chip design and the example of grating characterization is shown in Figure 4.2. The appearing of the ripples in the reflection curves indicates the existing of the reflection besides the grating. We checked the spacing of the ripple is corresponding to the distance between the MMI and the output port. Ripples in transmission curves were not observed may because the attenuation inside the polymer waveguide after the spiral structure is relative high so that the reflected from the TFF slot got attenuated.

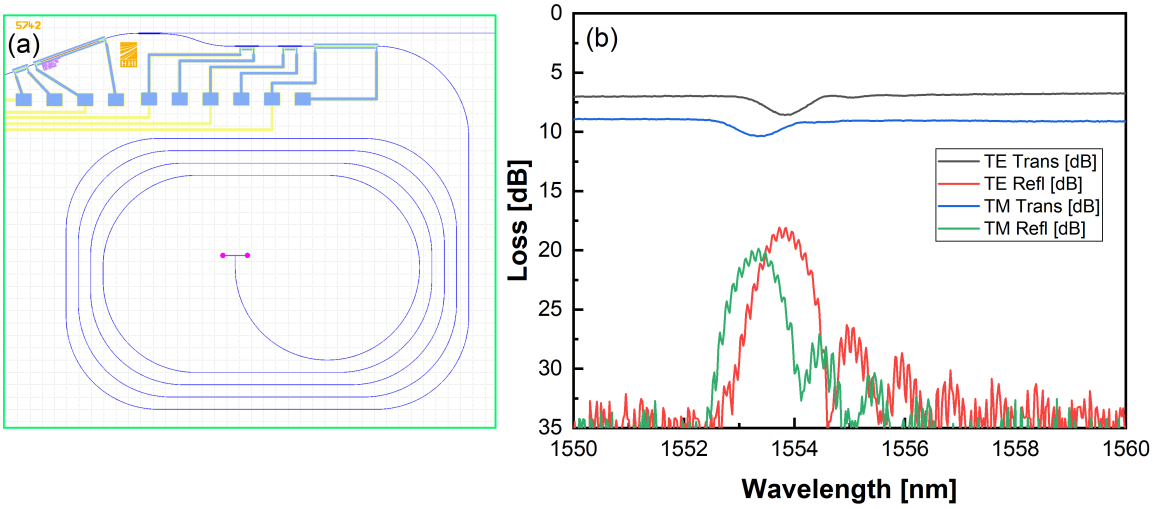

Figure 4.2.: (a) Chip design of the laser with long external cavity controllable feedback, (b) Grating characterization of the device, the spacing of the ripples in the reflection (red and green) curves are corresponding to the distance between MMI and output port.

4.1.3. Short Feedback Cavity

The on-chip short feedback cavity follows the same design principle as in Subsection 4.1.2, the chip design and the example of grating characterization is shown in Figure 4.4. In order to exploit PPR, Equation 2.17 is used to set the ideal cavity length. External cavity length of [3129.76, 3589,76, 3859.76, 4159.76, 4869.76, 5309.76, 6359.76] μm are choosen according to the FSR plot shown in Figure 4.3. Besides the simillar ripples in the reflection curves as in Figure 4.2, reflection is also observed in the transmission curves, with the spacing corresponding to the external cavity, which indicates the reflection from the TFF slot is relatively high in this case.

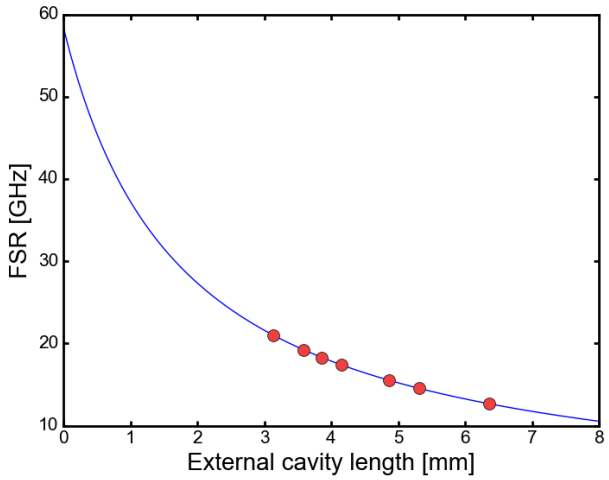

Figure 4.3.: FSR versus different external cavity length, the red circle markers are corresponding to the FSR of [22, 20, 19, 18, 16, 15, 13] GHz.

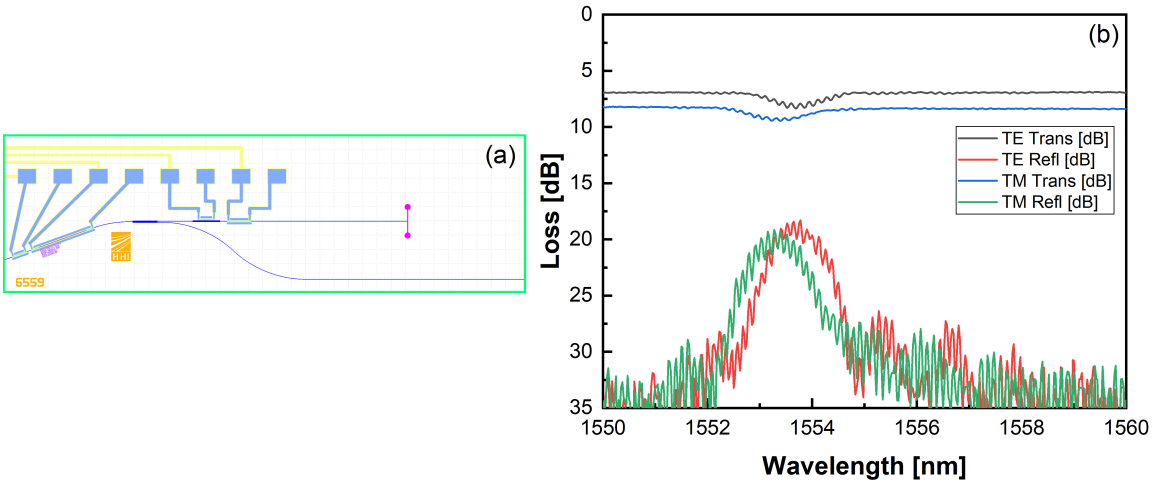

Figure 4.4.: (a) Chip design of the laser with short external cavity controllable feedback, (b) grating characterization of the device, the spacing of the ripples in the transmission (black and blue) and reflection (red and green) curves are corresponding to the length of the external cavity and the distance between MMI and output port respectively.

4.2. Characterization

Bandwidth enhancement by PPR is achieved with the short external cavity design. As shown in Figure 4.5, the appearing of the second resonance peak in the frequency response is clearly different from the ones we achieved in Figure 3.10.

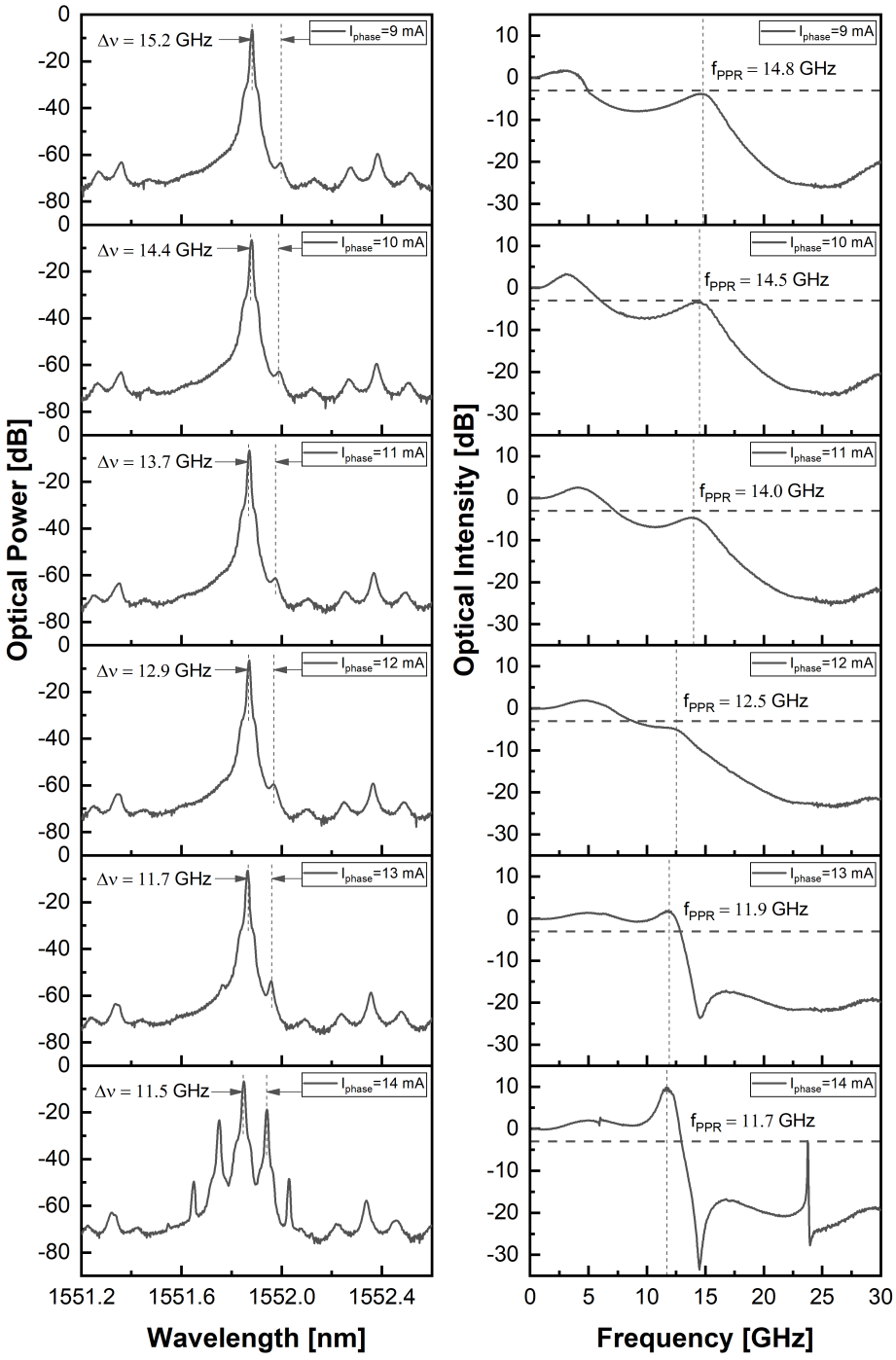

Figure 4.5.:

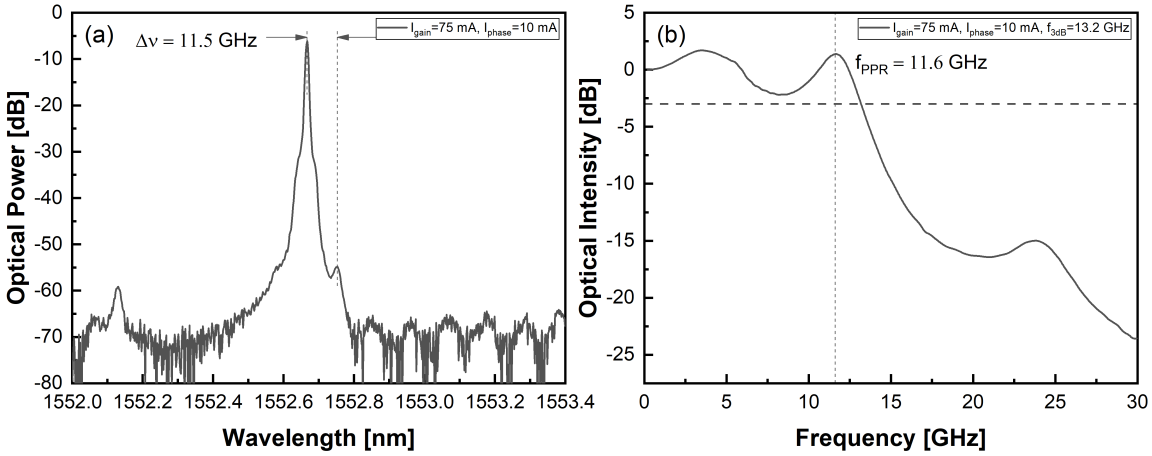

Figure 4.6.:

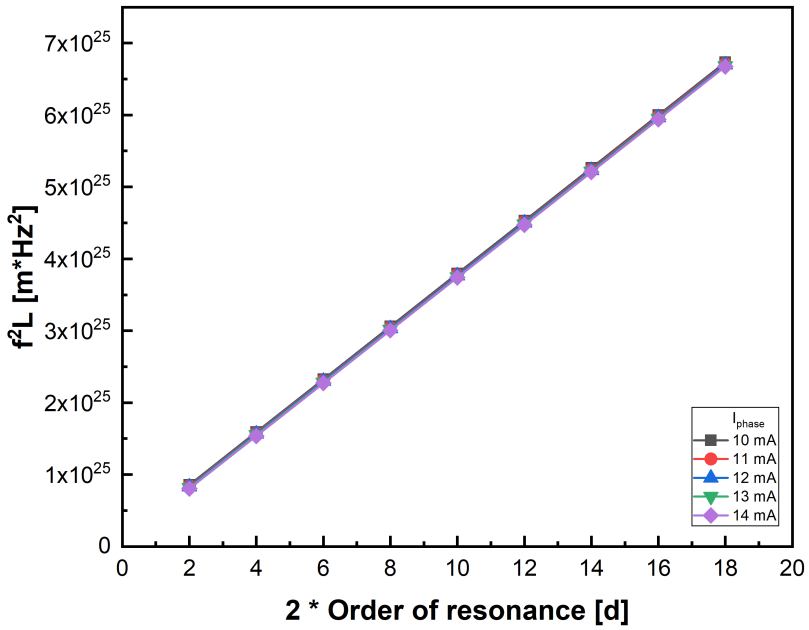

Figure 4.7.:

Table 4.1.: My caption

Current [mA]	α				
	$I_{phase} = 10\ mA$	$I_{phase} = 11\ mA$	$I_{phase} = 12\ mA$	$I_{phase} = 13\ mA$	$I_{phase} = 14\ mA$
75	1.725	2.063	2.22	2.624	3.247
75	1.818	1.991	2.296	2.618	3.257
75	1.818	2.07	2.246	2.614	3.253
75	1.808	2.054	2.242	2.566	3.221
Average	1.79225	2.0445	2.251	2.6055	3.2445

5. Conclusions & Outlook

5.1. Conclusions

5.2. Outlook

Bibliography

[1] Miguel C Soriano et al. "Complex photonics: Dynamics and applications of delay-coupled semiconductors lasers". In: *Reviews of Modern Physics* 85.1 (2013), p. 421.

[2] Mark Kuznetsov. "Theory of wavelength tuning in two-segment distributed feedback lasers". In: *IEEE journal of quantum electronics* 24.9 (1988), pp. 1837–1844.

[3] Daan Lenstra, B Verbeek, and A Den Boef. "Coherence collapse in single-mode semiconductor lasers due to optical feedback". In: *IEEE Journal of Quantum Electronics* 21.6 (1985), pp. 674–679.

[4] R Tkach and AR Chraplyvy. "Regimes of feedback effects in 1.5-μm distributed feedback lasers". In: *Journal of Lightwave technology* 4.11 (1986), pp. 1655–1661.

[5] Amnon Yariv and Michiharu Nakamura. "Periodic structures for integrated optics". In: *IEEE Journal of Quantum Electronics* 13.4 (1977), pp. 233–253.

[6] Marco Vallone, Paolo Bardella, and Ivo Montrosset. "Enhanced modulation bandwidth in complex cavity injection grating lasers". In: *IEEE Journal of Quantum Electronics* 47.10 (2011), pp. 1269–1276.

[7] Larry A Coldren, Scott W Corzine, and Milan L Mashanovitch. *Diode lasers and photonic integrated circuits*. Vol. 218. John Wiley & Sons, 2012.

[8] R Kazarinov and C Henry. "The relation of line narrowing and chirp reduction resulting from the coupling of a semiconductor laser to passive resonator". In: *IEEE Journal of quantum electronics* 23.9 (1987), pp. 1401–1409.

[9] Klaus Petermann. *Laser diode modulation and noise*. Vol. 3. Springer Science & Business Media, 2012.

[10] Kerry Vahala and Amnon Yariv. "Detuned loading in coupled cavity semiconductor lasers—effect on quantum noise and dynamics". In: *Applied Physics Letters* 45.5 (1984), pp. 501–503.

[11] Kerry Vahala, Joel Paslaski, and Amnon Yariv. "Observation of modulation speed enhancement, frequency modulation suppression, and phase noise reduction by detuned loading in a coupled-cavity semiconductor laser". In: *Applied Physics Letters* 46.11 (1985), pp. 1025–1027.

[12] Uwe Feiste. "Optimization of modulation bandwidth in DBR lasers with detuned Bragg reflectors". In: *IEEE journal of quantum electronics* 34.12 (1998), pp. 2371–2379.

[13] Olle Kjebon et al. "Two-section InGaAsP DBR-lasers at 1.55/spl mu/m wavelength with 31 GHz direct modulation bandwidth". In: *Indium Phosphide and Related Materials, 1997., International Conference on*. IEEE. 1997, pp. 665–668.

[14] Marek Chacinski and Richard Schatz. "Impact of losses in the Bragg section on the dynamics of detuned loaded DBR lasers". In: *IEEE Journal of Quantum Electronics* 46.9 (2010), pp. 1360–1367.

[15] Olle Kjebon et al. "Experimental evaluation of detuned loading effects on distortion in edge emitting DBR lasers". In: *IEEE International Topical Meeting on Microwave Photonics pp.* 2002, pp. 125–128.

[16] Junji Ohtsubo. *Semiconductor lasers: stability, instability and chaos*. Vol. 111. Springer, 2012.

[17] U Bandelow, HJ Wunsche, and H Wenzel. "Theory of selfpulsations in two-section DFB lasers". In: *IEEE photonics technology letters* 5.10 (1993), pp. 1176–1179.

[18] Richard Schatz et al. "Enhanced modulation bandwidth and self-pulsations in detuned loaded InGaAsP DBR-lasers". In: *Semiconductor Laser Conference, 1996., 15th IEEE International*. IEEE. 1996, pp. 93–94.

[19] Ivo Montrosset and Paolo Bardella. "Laser dynamics providing enhanced-modulation bandwidth". In: *Semiconductor Lasers and Laser Dynamics VI*. Vol. 9134. International Society for Optics and Photonics. 2014, 91340H.

[20] JP Reithmaier et al. "Modulation speed enhancement by coupling to higher order resonances: a road towards 40 GHz bandwidth lasers on InP". In: *Indium Phosphide and Related Materials, 2005. International Conference on*. IEEE. 2005, pp. 118–123.

[21] Alexei A Tager and Klaus Petermann. "High-frequency oscillations and self-mode locking in short external-cavity laser diodes". In: *IEEE Journal of Quantum Electronics* 30.7 (1994), pp. 1553–1561.

[22] Govind P Agrawal and Niloy K Dutta. *Semiconductor lasers*. Springer Science & Business Media, 2013.

[23] Asier Villafranca, Javier Lasobras, and Ignacio Garcés. "Precise characterization of the frequency chirp in directly modulated DFB lasers". In: *Electron Devices, 2007 Spanish Conference on*. IEEE. 2007, pp. 173–176.

[24] Christoph Harder, Kerry Vahala, and Amnon Yariv. "Measurement of the linewidth enhancement factor α of semiconductor lasers". In: *Applied Physics Letters* 42.4 (1983), pp. 328–330.

[25] F Devaux, Y Sorel, and JF Kerdiles. "Simple measurement of fiber dispersion and of chirp parameter of intensity modulated light emitter". In: *Journal of Lightwave Technology* 11.12 (1993), pp. 1937–1940.

[26] RC Srinivasan and JC Cartledge. "On using fiber transfer functions to characterize laser chirp and fiber dispersion". In: *IEEE Photonics Technology Letters* 7.11 (1995), pp. 1327–1329.

[27] Leif Bjerkan et al. "Measurement of laser parameters for simulation of high-speed fiberoptic systems". In: *Journal of Lightwave Technology* 14.5 (1996), pp. 839–850.

A. Appendix

chap:appendix

A.1. Photon-photon resonance calcuation